

**Clusters containing open-shell molecules. II. Equilibrium structures of Ar n OH Van der Waals clusters (X 2 Π, n=1 to 15)**

Minzhong Xu, Zlatko Bačić, and Jeremy M. Hutson

Citation: *The Journal of Chemical Physics* **117**, 4777 (2002); doi: 10.1063/1.1497966

View online: <http://dx.doi.org/10.1063/1.1497966>

View Table of Contents: <http://scitation.aip.org/content/aip/journal/jcp/117/10?ver=pdfcov>

Published by the [AIP Publishing](#)

---

**Articles you may be interested in**

[Ar n HF van der Waals clusters revisited. I. New low-energy isomeric structures for n=6–13](#)  
*J. Chem. Phys.* **121**, 11045 (2004); 10.1063/1.1811612

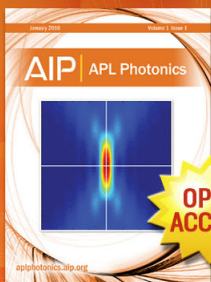
[Jahn–Teller effect in van der Waals complexes; Ar–C 6 H 6 + and Ar–C 6 D 6 +](#)  
*J. Chem. Phys.* **120**, 10069 (2004); 10.1063/1.1714793

[Microwave spectrum, structure, and internal motion of the open-shell van der Waals complex Ar–ClO 2](#)  
*J. Chem. Phys.* **119**, 8404 (2003); 10.1063/1.1612921

[Clusters containing open-shell molecules. III. Quantum five-dimensional/two-surface bound-state calculations on Ar n OH van der Waals clusters \(X 2 Π, n=4 to 12\)](#)  
*J. Chem. Phys.* **117**, 4787 (2002); 10.1063/1.1497967

[Nonadditive intermolecular forces in Ar n –HF van der Waals clusters: Effects on the HF vibrational frequency shift](#)  
*J. Chem. Phys.* **111**, 8378 (1999); 10.1063/1.480179

---



Launching in 2016!

The future of applied photonics research is here

**OPEN  
ACCESS**

**AIP** | APL  
Photonics

## Clusters containing open-shell molecules. II. Equilibrium structures of $\text{Ar}_n\text{OH}$ Van der Waals clusters ( $X^2\Pi$ , $n=1$ to 15)

Minzhong Xu and Zlatko Bačić<sup>a)</sup>

*Department of Chemistry, New York University, New York, New York 10003*

Jeremy M. Hutson<sup>b)</sup>

*Department of Chemistry, University of Durham, South Road, Durham, DH1 3LE, England*

(Received 1 May 2002; accepted 12 June 2002)

The equilibrium and low-lying isomeric structures of  $\text{Ar}_n\text{OH}$  ( $X^2\Pi$ ) clusters for  $n=1$  to 15 are investigated by simulated annealing calculations. Potential energy surfaces are obtained by a pairwise-additive approach, taking into account the open-shell nature of OH  $X^2\Pi$  and including spin-orbit coupling. It is found that the spin-orbit coupling suppresses the Jahn–Teller effect, and many of the clusters have high-symmetry structures ( $C_{nv}$  with  $n>2$ ) which would be forbidden in the absence of spin-orbit coupling. The structures are generally similar to those previously found for the closed-shell systems  $\text{Ar}_n\text{HF}$  and  $\text{Ar}_n\text{HCl}$ , but different from those for the open-shell systems  $\text{Ar}_n\text{NO}$  and  $\text{Ar}_n\text{CH}$ . This is because Ar–OH ( $X^2\Pi$ ), like Ar–HF and Ar–HCl but unlike Ar–NO and Ar–CH, has a near-linear equilibrium structure.  $\text{Ar}_n\text{OH}$  clusters for  $n$  up to 6 have all Ar atoms in a single shell around OH. In the clusters with  $n=7$  to 9, OH is under a pentagonal pyramid formed by six Ar atoms, while the others bind to its exterior, away from OH. For  $n=10$  to 12, the minimum-energy structures have OH inside an  $\text{Ar}_n$  cage, which is essentially icosahedral for  $n=12$  but has vacancies for  $n=10$  and 11. For  $n>12$ , the extra Ar atoms begin to form a second solvation shell. The global minimum of  $\text{Ar}_n\text{OH}$  may be constructed from the minimum-energy structure of  $\text{Ar}_{n+1}$  by replacing one Ar atom with OH. © 2002 American Institute of Physics. [DOI: 10.1063/1.1497966]

### I. INTRODUCTION

Studies of Van der Waals complexes and clusters can provide an understanding of additive and nonadditive contributions to potential energy surfaces, and thus provide a firm foundation for the study of condensed phases. The understanding that can be gained is exemplified by complexes and clusters formed between HF and Ar. In the period 1981–1991, extensive high-resolution spectra of the Ar–HF and Ar–DF Van der Waals complexes were observed in the microwave,<sup>1–3</sup> far-infrared,<sup>4</sup> and mid-infrared<sup>5–8</sup> regions of the spectrum. Then, in 1992, Hutson<sup>9</sup> used the spectra in a combined least-squares fit to obtain an accurate and reliable model of the Ar–HF pair potential. The resulting potential included a parametric dependence on the HF vibrational quantum number  $v$ , as well as explicit dependence on the intermolecular distance  $R$  and angle  $\theta$ .

High-resolution microwave,<sup>10</sup> mid-infrared,<sup>11–13</sup> and near-infrared<sup>14</sup> spectra of  $\text{Ar}_2\text{–HF}$  and  $\text{Ar}_2\text{–DF}$  were also measured. Ernesti and Hutson<sup>15</sup> showed that pairwise-additive potential surfaces built using the Ar–HF and Ar–Ar pair potentials could give a good qualitative account of these spectra, but that nonadditive terms were needed to reproduce the spectra quantitatively. Accordingly, the trimer spectra were used to develop models for the nonadditivity.<sup>15,16</sup> It was found that novel nonadditive terms, arising from the interac-

tion of the HF permanent multipole moments with overlap-induced multipoles on the Ar atoms, were needed to describe the spectra.

In parallel work, Bačić and co-workers carried out calculations on  $\text{Ar}_n\text{HF}$  clusters with  $n>2$ , initially using pairwise-additive potential energy surfaces.<sup>17</sup> They focused on the calculation of infrared frequency shifts for  $\text{Ar}_n\text{HF}$  clusters with  $n=3–14$ , by performing calculations on effective Ar–HF potentials corresponding to HF in its  $v=0$  and 1 states. Their calculations were of three distinct types: (i) simulated annealing, which located global and low-lying local minima on the potential energy surfaces;<sup>18</sup> (ii) five-dimensional (5D) quantum bound-state calculations,<sup>19–21</sup> in which the HF molecule was allowed to translate and rotate against or inside a fixed  $\text{Ar}_n$  subunit or cage, which was fixed at the geometry of one of the minima; and (iii) full-dimensional quantum bound-state calculations, using a diffusion Monte Carlo approach (DMC), in which the Ar cage was allowed to vibrate.<sup>22</sup> The full-dimensional calculations were initially carried out only for  $n\leq 4$  and for the ground state of the intermolecular vibrational motion. The general conclusions from these calculations were (i) that the 5D calculations captured the essential physics necessary for the calculation of frequency shifts; and (ii) that the pairwise-additive potentials were a good starting point, but that there were remaining discrepancies of about 10% between the experimental results and the pairwise frequency shifts. Very recently, the DMC calculations of the zero-point energies and vibrational frequency shifts, for pairwise-additive poten-

<sup>a)</sup> Author to whom correspondence should be addressed. Electronic mail: zlatko.bacic@nyu.edu

<sup>b)</sup> Electronic mail: j.m.hutson@durham.ac.uk

tial energy surfaces, have been extended to the low-lying isomers of  $\text{Ar}_n\text{HF}$  clusters with  $n \leq 7$  and  $n = 12$ .<sup>23</sup>

In a recent development, the work on nonadditive forces<sup>15,16</sup> and on cluster structure and dynamics<sup>18–22</sup> has been brought together, and the nonadditive models developed for  $\text{Ar}_2\text{HF}$  have been applied to larger  $\text{Ar}_n\text{HF}$  clusters.<sup>24</sup> The nonadditive potentials were found to account remarkably well for the frequency shifts for  $n = 3$  and  $n = 4$ ,<sup>24</sup> which were the largest  $\text{Ar}_n\text{HF}$  clusters that had then been observed.<sup>11,25</sup> However, Nauta and Miller<sup>26</sup> have succeeded recently in preparing size-selected  $\text{Ar}_n\text{HF}$  clusters in liquid helium droplets for  $n$  up to 9, and in observing multiple structural isomers for  $n > 3$ . They were able to make unambiguous assignments of all the clusters they observed, on the basis of the quantum 5D calculations of the frequency shifts on the pairwise-additive potential energy surfaces.<sup>20,21</sup> For  $n = 4$ , they confirmed that the nonadditive calculations<sup>24</sup> give good agreement with experiment for the second minimum structure as well as for the absolute minimum. The nonadditive shifts have not yet been calculated for clusters with  $n > 4$ , but this would be very interesting.

The present work begins an effort to obtain a similar understanding for clusters containing OH ( $X^2\Pi$ ), which is a prototype open-shell molecule. The parent complex  $\text{Ar-OH}$  has been the object of intensive experimental study by laser-induced fluorescence (LIF),<sup>27–30</sup> stimulated emission pumping (SEP),<sup>31–33</sup> microwave spectroscopy,<sup>34</sup> and most recently by direct infrared absorption<sup>35</sup> in supersonic jets. The spectra up to 1993 were used by Dubernet and Hutson<sup>36</sup> to obtain a potential energy surface for  $\text{Ar-OH}$  ( $X^2\Pi$ ).

Clusters containing open-shell molecules are particularly interesting because they are models for the solvation of reactive species and reaction intermediates. The range of structures available for such clusters is considerably richer even than for clusters such as  $\text{Ar}_n\text{HF}$ .<sup>18</sup> In previous work, we have explored the structures of  $\text{Ar}_n\text{CH}$  clusters<sup>37</sup> (Paper I) by performing simulated annealing calculations on surfaces that take account of the open-shell character and include spin-orbit coupling. In the present work, this will be extended to  $\text{Ar}_n\text{OH}$  clusters, in order to find their global and local minimum structures. In a companion paper,<sup>38</sup> we will develop the theory needed to carry out the analog of quantum five-dimensional bound-state calculations on  $\text{Ar}_n\text{OH}$  clusters, including both potential energy surfaces that correlate with OH ( $X^2\Pi$ ).

## II. METHODOLOGY

### A. Potential energy surfaces for a molecule in a $\Pi$ state interacting with $n$ closed-shell atoms

The interaction potential between a molecule in a  $\Pi$  state and a single closed-shell atom is usually characterized by two potential energy surfaces,  $V_{A'}(R, \theta)$  and  $V_{A''}(R, \theta)$ . The corresponding electronic wave functions are even and odd, respectively, with respect to reflection in the plane of the molecule, so that the two surfaces correspond to the approach of the atom along a lobe of the singly occupied  $\pi$  orbital, or in its nodal plane, respectively.

In a cluster containing a molecule in a  $\Pi$  state and  $n$

perturbing closed-shell atoms, there are still two potential energy surfaces. However, these cannot be obtained by summing the atom-diatom potentials  $V_{A'}$  and  $V_{A''}$  directly, because there is in general no single molecular plane. Under these circumstances, it is easier to work with the sum and difference potentials,

$$V_0(R, \theta) = \frac{1}{2}[V_{A'}(R, \theta) + V_{A''}(R, \theta)], \quad (1)$$

$$V_2(R, \theta) = \frac{1}{2}[V_{A'}(R, \theta) - V_{A''}(R, \theta)]. \quad (2)$$

The potentials  $V_\nu(R, \theta)$  ( $\nu = 0, 2$ ) may be thought of as the components in an expansion

$$V(R, \theta, \chi) = \sum_\nu V_\nu(R, \theta) \exp(i\nu\chi), \quad (3)$$

where  $\chi$  is an angle that describes the azimuthal position of the unpaired electron with respect to the triatomic plane. This viewpoint is useful in understanding the matrix elements between electronic functions.

In a basis set of orbital functions with diatom angular momentum  $\lambda = +1$  and  $-1$ , the potential due to the interaction of  $n$  Ar atoms with OH ( $X^2\Pi$ ),  $\mathbf{V}_{\text{Ar-CH}}^{\text{tot}}$ , can be represented by a  $2 \times 2$  matrix

$$\mathbf{V}_{\text{Ar-OH}}^{\text{tot}} = \begin{pmatrix} V_0^{\text{tot}} & V_2^{\text{tot}} \\ (V_2^{\text{tot}})^* & V_0^{\text{tot}} \end{pmatrix}. \quad (4)$$

In this basis set,  $V_0$  is diagonal and  $V_2$  provides an off-diagonal matrix element of magnitude  $V_2$  for each perturbing atom. The quantities  $V_0^{\text{tot}}$  and  $V_2^{\text{tot}}$  will be defined in more detail below.

When there are several perturbing atoms, the matrix elements of the potential are most conveniently calculated in a monomer-fixed axis system with its  $z$  axis along the OH bond and its  $x$  axis containing one of the solvating atoms. The positions of the  $n$  perturbing atoms are specified by spherical polar coordinates  $R_i$ ,  $\theta_i$ ,  $\chi_i$  for  $i = 1-n$ . In the present model, we take the part of the potential that is diagonal in  $\lambda$ , due to  $V_0$ , to be just a simple sum over  $n$  atomic perturbers,

$$V_0^{\text{tot}} = \langle +1 | V | +1 \rangle = \langle -1 | V | -1 \rangle = \sum_{i=1}^n V_0(R_i, \theta_i). \quad (5)$$

However, the off-diagonal terms, due to the difference potential  $V_2$ , depend on  $\chi_i$ ,

$$V_2^{\text{tot}} = \langle +1 | V | -1 \rangle = \langle -1 | V | +1 \rangle^* \\ = \sum_{i=1}^n V_2(R_i, \theta_i) \exp(-2i\chi_i). \quad (6)$$

The exponential factor in Eq. (6) arises because the potential due to atom  $i$  actually contains factors  $\exp(i\nu(\chi - \chi_i))$  instead of  $\exp(i\nu\chi)$ . Because of the phase factors, the overall effect of  $V_2$  vanishes for any regular array of atoms with more than twofold symmetry around the  $z$  axis. In general, however,  $V_2^{\text{tot}}$  as defined here is a complex quantity, and the matrix (4) is complex Hermitian rather than real symmetric.

The interaction potential between  $n$  Ar atoms,  $\mathbf{V}_{\text{Ar-Ar}}^{\text{tot}}$ , is also taken to be pairwise additive in the present model,

$$V_{\text{Ar-Ar}}^{\text{tot}} = \sum_{i < j}^n V_{\text{Ar-Ar}}(R_{ij}), \quad (7)$$

where  $R_{ij}$  is the distance between Ar atoms  $i$  and  $j$ .

Diagonalizing the matrix (4) and adding the Ar–Ar contribution (7) would give the two adiabatic potential energy surfaces for the  $\text{Ar}_n\text{OH}$  cluster in the absence of spin-orbit coupling. For the case of a single Ar atom, it would return the original  $A'$  and  $A''$  surfaces. However, spin-orbit coupling provides additional matrix elements, and it is preferable to include them in defining the effective potentials for geometry optimization. In the basis set of functions with  $\lambda = +1$  and  $-1$ , the spin-orbit matrix is

$$\mathbf{H}_{\text{so}} = \begin{pmatrix} a_v/2 & 0 \\ 0 & -a_v/2 \end{pmatrix} \quad (8)$$

for spin projection quantum number  $\sigma = +\frac{1}{2}$ . The spin-orbit coupling constant  $a_v$  is taken to be  $-139.21 \text{ cm}^{-1}$  for the  $v=0$  vibrational level of OH ( $X^2\Pi$ ),<sup>39</sup> and is assumed to be unaffected by the presence of Ar atoms. In the present work, we diagonalize the  $2 \times 2$  matrix  $\mathbf{V}_{\text{Ar-OH}}^{\text{tot}} + \mathbf{H}_{\text{so}}$ . We then add the Ar–Ar contribution (7) and use the *lower* of the two resulting surfaces to find the structure of the global minimum and low-lying structural isomers. In an accompanying paper,<sup>38</sup> we will investigate the dynamics of  $\text{Ar}_n\text{OH}$  ( $X^2\Pi$ ) clusters considering *both* surfaces and the coupling between them.

It is worth noting that including the spin-orbit contribution (8) reduces the influence of the Jahn–Teller effect on the structures. In the absence of spin-orbit coupling,  $V_2^{\text{tot}}$  mixes two *degenerate* states. If the geometry is a symmetrical one where  $V_2$  vanishes because of the phase factors in Eq. (6), the Jahn–Teller effect will always cause the cluster to distort to resolve the degeneracy. However, this is not the case when spin-orbit coupling is included, because the states with  $\lambda = +1$  and  $-1$  are no longer degenerate when  $V_2^{\text{tot}}$  is zero.

## B. Ar–OH and Ar–Ar potentials

In the present work, we use potential energy surfaces constructed from the Ar–OH ( $X^2\Pi$ ) surfaces of Dubernet and Hutson,<sup>36</sup> assuming pairwise additivity in the sense of Eqs. (5) and (6). It may be noted that the phase factors in Eq. (6) actually make the surface nonadditive in the usual sense.

The sum and difference potentials for Ar–OH<sup>36</sup> were obtained by fitting to experimental data from stimulated-emission pumping (SEP)<sup>33</sup> and microwave<sup>34</sup> spectra of the Ar–OH complex. All the experimental data were for OH in its  $v=0$  vibrational state, so that the resulting  $V_0(R, \theta)$  and  $V_2(R, \theta)$  are effective two-dimensional potentials for this state. Contour plots of  $V_0$  and  $V_2$  for Ar–OH are shown in Fig. 1;  $\theta$  is  $0^\circ$  at the linear Ar–OH geometry and  $180^\circ$  at the linear Ar–OH configuration. The  $V_0$  potential has a global minimum that is  $125.93 \text{ cm}^{-1}$  deep, at a near-linear Ar–OH geometry with  $\theta = 13^\circ$  and  $R = 3.65 \text{ \AA}$ . A secondary minimum exists at the collinear Ar–OH geometry, for  $\theta = 180^\circ$  and  $R = 3.48 \text{ \AA}$ , which has a well depth of  $106.3 \text{ cm}^{-1}$ . The two minima are displayed in Fig. 2.

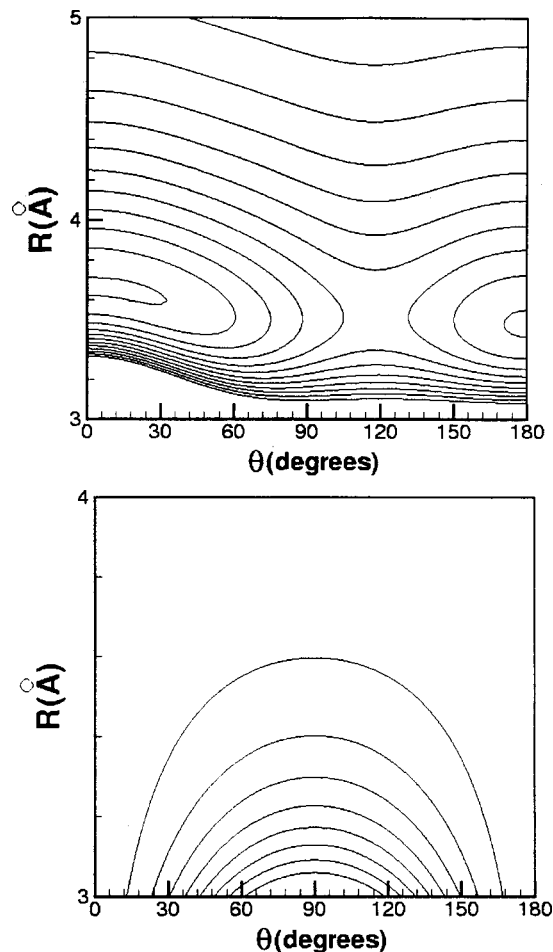


FIG. 1. Contour plots of the 2D potential energy surfaces  $V_0$  (top) and  $V_2$  (bottom) for Ar–OH ( $X^2\Pi$ ).  $\theta = 0^\circ$  corresponds to the linear Ar–HO geometry, and  $\theta = 180^\circ$  to the linear Ar–OH geometry. In the top figure, the lowest-energy contour is at  $-125 \text{ cm}^{-1}$  and interval between the contours is  $10 \text{ cm}^{-1}$ . In the bottom figure, the innermost contour is at  $75 \text{ cm}^{-1}$ , with the interval between the contours of  $-10 \text{ cm}^{-1}$ ;  $V_2$  decreases from the innermost contour to the outer contours.

The Ar–Ar interaction potential used in the present work is the HFD-C potential of Aziz and Chen,<sup>40</sup> which has a well depth of  $99.55 \text{ cm}^{-1}$  at an equilibrium Ar–Ar distance of  $3.759 \text{ \AA}$ .

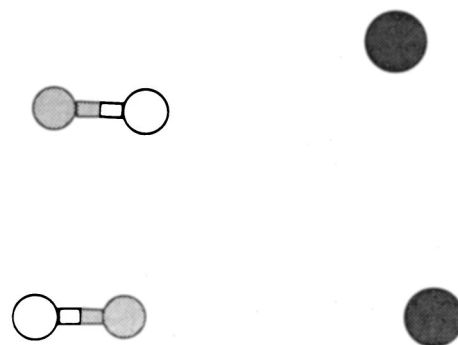


FIG. 2. Calculated isomeric structures of Ar–OH: (top) minimum-energy (ME) structure ( $V_{1,1}$ ); (bottom) next higher isomer ( $V_{1,2}$ , ME+19.60  $\text{cm}^{-1}$ ). Their energies are given in Table I.

TABLE I. Calculated global and low-lying local minima for  $\text{Ar}_n\text{OH}$  ( $X^2\Pi$ ) clusters with  $n=1-15$ .  $V_{n,i}$  represents the  $i$ th minimum of the cluster of size  $n$ . The energies of the minima (in  $\text{cm}^{-1}$ ) are relative to OH in its lowest spin-orbit state  $^2\Pi_{3/2}$  and  $n$  separated Ar atoms.

$n$	$V_{n,1}$	$V_{n,2}$	$V_{n,3}$	$V_{n,4}$	$V_{n,5}$
1	-125.928	-106.332			
2	-349.941	-235.377			
3	-671.478	-568.915	-463.684		
4	-989.703	-979.725	-875.458	-790.360	
5	-1346.256	-1309.453	-1303.661	-1293.059	
6	-1725.744	-1713.905	-1661.019	-1657.131	-1641.773
7	-2047.568	-2043.807	-2038.830	-2035.167	-2034.291
8	-2465.718	-2448.310	-2446.526	-2444.638	-2375.947
9	-2878.705	-2866.924	-2858.313	-2852.988	-2795.885
10	-3307.451	-3291.318	-3289.374	-3286.938	-3279.814
11	-3827.008	-3770.466	-3761.266	-3752.873	-3738.810
12	-4447.754	-4361.464	-4160.939	-4159.702	-4158.160
13	-4782.719	-4719.171			
14	-5209.920	-5150.837	-5134.041		
15	-5636.523	-5573.355	-5567.292		

### C. Optimization of cluster geometries

The global and low-lying local minima of  $\text{Ar}_n\text{OH}$  ( $X^2\Pi$ ) reported here were obtained using the same methodology as in our earlier work on  $\text{Ar}_n\text{HF}$ ,<sup>18</sup>  $\text{Ar}_n\text{H}_2\text{O}$ ,<sup>41</sup> and  $\text{Ar}_n\text{CH}$ <sup>37</sup> clusters. The geometries of  $\text{Ar}_n\text{OH}$  clusters were first optimized by means of simulated annealing, and subsequently refined by a direct minimization scheme using several Newton–Raphson steps. For larger clusters, the Cerjan–Miller eigenvector-following method<sup>42,43</sup> was used to verify these results, and to check that the simulated annealing did not miss any of the cluster minima.

## III. RESULTS AND DISCUSSION

The computational methodology outlined in Sec. II was used to determine the minimum-energy structures and low-lying isomers of  $\text{Ar}_n\text{OH}$  ( $X^2\Pi$ ) clusters for  $n=1-15$ . The symbol  $V_{n,i}$  designates the energy of the  $i$ th minimum of the cluster with  $n$  Ar atoms, and  $i=1$  indicates the global minimum. The energies of the global and local minima of  $\text{Ar}_n\text{OH}$  ( $X^2\Pi$ ) clusters are listed in Table I; they are given relative to OH in its lowest spin-orbit state  $^2\Pi_{3/2}$  and  $n$  Ar atoms at infinite separation. In the following, we discuss the main features of the cluster structures, identify the major trends in their size evolution, and make comparisons with some other molecule-doped heteroclusters.

### A. The minimum-energy cluster structures and low-lying isomers

#### 1. $\text{Ar}_2\text{OH}$

The structures corresponding to the two lowest minima of  $\text{Ar}_2\text{OH}$  are shown in Fig. 3. The minimum-energy structure ( $C_{2v}$ ) is T-shaped, with OH on the  $C_2$  axis, and its H atom pointing towards the  $\text{Ar}_2$  subunit. The next higher isomer,  $114.6 \text{ cm}^{-1}$  above the global minimum, has the two Ar atoms at positions corresponding to the global and the local minimum, respectively, of Ar–OH (Fig. 2).

It is instructive to compare the equilibrium geometry of  $\text{Ar}_2\text{OH}$  ( $X^2\Pi$ ) with those of  $\text{Ar}_2\text{NO}$  ( $X^2\Pi$ ) and  $\text{Ar}_2\text{CH}$  ( $X^2\Pi$ ) open-shell clusters, which have been studied recently.

The minimum-energy structure of  $\text{Ar}_2\text{NO}$  is bent,<sup>44</sup> with both Ar atoms occupying T-shaped positions, despite the fact that, like OH ( $X^2\Pi$ ), the  $X^2\Pi$  state of NO has a  $\pi^3$  configuration. This difference in equilibrium geometries arises because the equilibrium structure of  $\text{ArNO}$  is T-shaped, by contrast to that of  $\text{ArOH}$ , which is near-linear. The energetically optimal structure of  $\text{Ar}_2\text{CH}$  is very different from the global minima of either  $\text{Ar}_2\text{OH}$  or  $\text{Ar}_2\text{NO}$ ; all four atoms are in the same plane, with the two Ar atoms in the T-shaped configuration relative to CH.<sup>37</sup> Because of the  $\pi^1$  configuration of CH ( $X^2\Pi$ ), the Ar–CH interaction potential strongly favors approach of an Ar atom in the nodal plane of the singly occupied  $\pi$  orbital;<sup>45</sup> this preference gives rise to coplanar  $\text{Ar}_2\text{CH}$ , with the two Ar atoms on opposite sides of CH. The coplanar  $\text{Ar}_2\text{CH}$  motif was found to persist in larger  $\text{Ar}_n\text{CH}$  clusters, strongly distorting their Ar cages.<sup>37</sup>

Interestingly, it is the equilibrium geometries of the closed-shell clusters  $\text{Ar}_2\text{HF}$ <sup>18</sup> and  $\text{Ar}_2\text{HCl}$ <sup>46</sup> that are the most

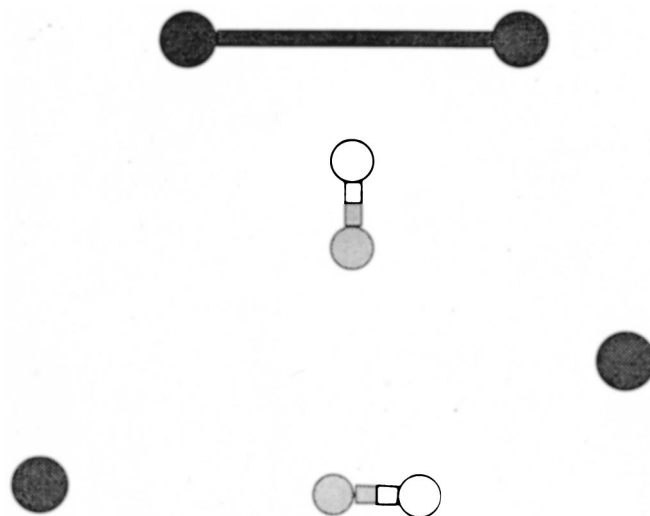


FIG. 3. Calculated isomeric structures of  $\text{Ar}_2\text{OH}$ : (top) minimum-energy (ME) structure ( $V_{2,1}$ ); (bottom) next higher isomer ( $V_{2,2}$ ), ME+114.56  $\text{cm}^{-1}$ . Their energies are given in Table I.

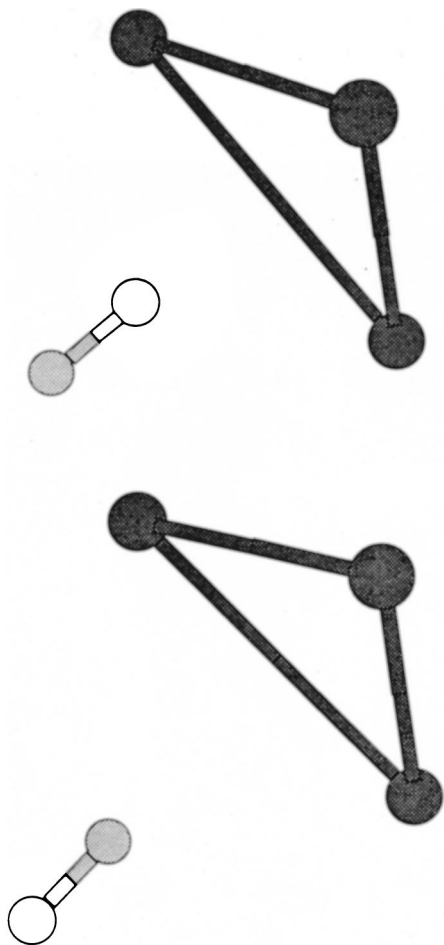


FIG. 4. Calculated isomeric structures of  $\text{Ar}_3\text{OH}$ : (top) minimum-energy (ME) structure ( $V_{3,1}$ ); (bottom) next higher isomer ( $V_{3,2}$ ),  $\text{ME}+102.56\text{ cm}^{-1}$ . Their energies are given in Table I.

similar to that of  $\text{Ar}_2\text{OH}$ . This similarity arises (a) because all three  $\text{Ar-HX}$  ( $X=\text{F,Cl,O}$ ) potential energy surfaces have global minima at or near the collinear  $\text{Ar-HX}$  geometry, and (b) because of the  $\pi^3$  configuration of OH ( $X^2\Pi$ ), the  $\text{Ar-OH}$  interaction potential does not vary much between in-plane and out-of-plane approach of an Ar atom. It therefore does not deviate appreciably from the cylindrical symmetry which characterizes the interaction of Ar with closed-shell diatomics.

## 2. $\text{Ar}_n\text{OH}$ , $n=3-5$

The minimum-energy structure and the next higher isomer of  $\text{Ar}_3\text{OH}$ , displayed in Fig. 4, are separated by  $102.6\text{ cm}^{-1}$ . Both configurations have  $C_{3v}$  symmetry, and differ only in the orientation of the OH monomer; the global minimum has the H atom pointing towards the  $\text{Ar}_3$  plane, while in the local minimum it is the O atom which faces the  $\text{Ar}_3$  subunit.

The global ( $C_{2v}$ ) and the next higher minimum ( $C_{3v}$ ) of  $\text{Ar}_4\text{OH}$  (Fig. 5) are only  $10\text{ cm}^{-1}$  apart. In the  $C_{2v}$  structure, the four Ar atoms are in a “folded diamond” arrangement, and in the  $C_{3v}$  isomer they form a tetrahedron.

The two lowest-lying isomers of  $\text{Ar}_5\text{OH}$  are shown in Fig. 6. The minimum-energy structure ( $C_{4v}$ ) has a square

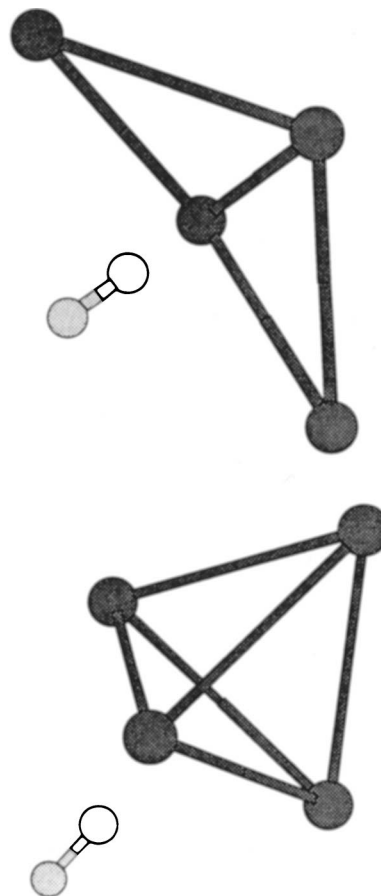


FIG. 5. Calculated isomeric structures of  $\text{Ar}_4\text{OH}$ : (top) minimum-energy (ME) structure ( $V_{4,1}$ ); (bottom) next higher isomer ( $V_{4,2}$ ),  $\text{ME}+9.98\text{ cm}^{-1}$ . Their energies are given in Table I.

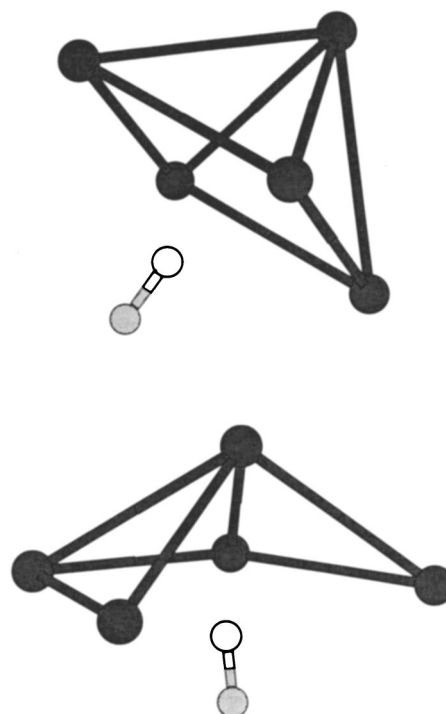


FIG. 6. Calculated isomeric structures of  $\text{Ar}_5\text{OH}$ : (top) minimum-energy (ME) structure ( $V_{5,1}$ ); (bottom) next higher isomer ( $V_{5,2}$ ),  $\text{ME}+36.80\text{ cm}^{-1}$ . Their energies are given in Table I.

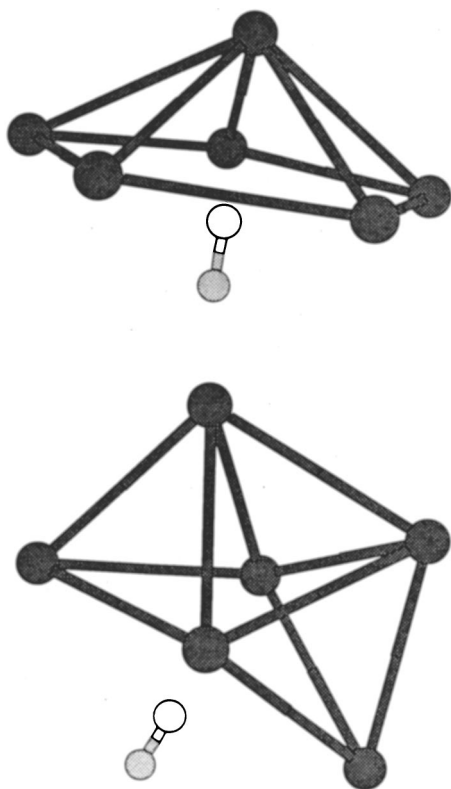


FIG. 7. Calculated isomeric structures of  $\text{Ar}_6\text{OH}$ : (top) minimum-energy (ME) structure ( $V_{6,1}$ ); (bottom) next higher isomer ( $V_{6,2}$ ),  $\text{ME}+11.84 \text{ cm}^{-1}$ . Their energies are given in Table I.

pyramid of Ar atoms; OH is located below the pyramid on the  $C_4$  axis, its H atom facing the base of the pyramid. The next higher isomer of  $\text{Ar}_5\text{OH}$  [Fig. 6 (bottom)],  $36.8 \text{ cm}^{-1}$  above the global minimum, arises by adding one Ar atom to an edge of the energetically optimal configuration of  $\text{Ar}_4\text{OH}$  in Fig. 5 (top).

The equilibrium geometries of  $\text{Ar}_n\text{OH}$  for  $n=3-5$  are virtually identical to those of  $\text{Ar}_n\text{HCl}$  clusters of the same size.<sup>46</sup> Strong similarity also exists with the minimum-energy structures of the corresponding  $\text{Ar}_n\text{NO}$  clusters,<sup>44</sup> with one notable difference: while OH is aligned along the rotational symmetry axis of the cluster, NO lies nearly parallel to the  $\text{Ar}_n$  subunit.

It should be noted that the high-symmetry structures ( $C_{nv}$  with  $n>2$ ) can exist only because the spin-orbit coupling quenches the Jahn–Teller effect as described above. If the same potential energy surfaces were used for a cluster containing a  $^1\Pi$  molecule, or spin-orbit coupling was neglected, the high-symmetry structures would distort to resolve the electronic degeneracy.

Finally, it is useful to point out here that, in general, the lowest-energy configurations of these and larger  $\text{Ar}_n\text{OH}$  clusters ( $n\geq 6$ , see below) can be related to the global minima of pure  $\text{Ar}_{n+1}$  clusters (tetrahedron for  $\text{Ar}_4$ , trigonal bipyramid for  $\text{Ar}_5$ , octahedron for  $\text{Ar}_6$ , etc.),<sup>18,47,48</sup> with OH playing the role of an Ar atom and its H-atom end pointing towards  $\text{Ar}_n$ . The only exception is  $\text{Ar}_4\text{OH}$ , where the  $C_{3v}$  structure [Fig. 5 (bottom)] derived from the global minimum

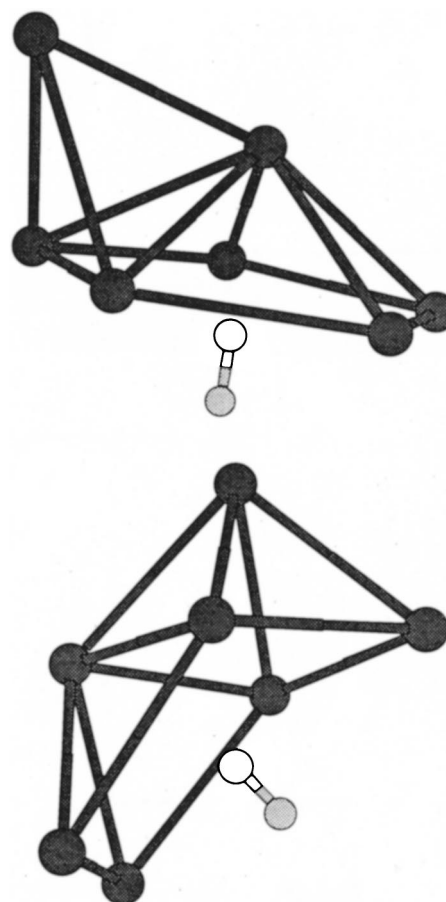


FIG. 8. Calculated isomeric structures of  $\text{Ar}_7\text{OH}$ : (top) minimum-energy (ME) structure ( $V_{7,1}$ ); (bottom) next higher isomer ( $V_{7,2}$ ),  $\text{ME}+3.76 \text{ cm}^{-1}$ . Their energies are given in Table I.

of  $\text{Ar}_5$ , the trigonal bipyramid, is less stable by  $10 \text{ cm}^{-1}$  than the  $C_{2v}$  structure in Fig. 5 (top).

The same relationship with  $\text{Ar}_{n+1}$  holds for  $\text{Ar}_n\text{NO}$  clusters,<sup>44</sup> and was observed earlier for some cluster sizes of  $\text{Ar}_n\text{HF}$ <sup>18</sup> and  $\text{Ar}_n\text{H}_2\text{O}$ .<sup>41</sup>

### 3. $\text{Ar}_n\text{OH}$ , $n=6-9$

In the minimum-energy structure of  $\text{Ar}_6\text{OH}(C_{5v})$ , displayed in Fig. 7 (top), the Ar atoms adopt the configuration of a pentagonal pyramid, with OH under the pyramid and the H atom facing its base. As discussed below, the pentagonal pyramid motif is the key building block for the equilibrium structures of larger  $\text{Ar}_n\text{OH}$  clusters with  $n>6$ . The  $\text{Ar}_6\text{OH}$  global minimum can be derived from that of pure  $\text{Ar}_7$  (pentagonal bipyramid),<sup>18,47,48</sup> by replacing the “bottom” axial Ar with OH. The closest local minimum, corresponding to the  $C_{2v}$  structure shown in Fig. 7 (bottom), is  $11.8 \text{ cm}^{-1}$  higher in energy. The six Ar atoms form three fused tetrahedra, resulting in a polytetrahedral configuration.<sup>18,47,48</sup>

The energetically optimal structures for clusters with  $n=7-9$ , shown in Figs. 8–10 (top), are built upon that for  $n=6$  [Fig. 7 (top)]. The additional Ar atoms bind to the triangular faces on the exterior of the  $\text{Ar}_6$  pyramid, in effect forming a partial second solvation shell around OH. The equilibrium geometries of  $\text{Ar}_n\text{OH}$  for  $n=6-9$  are again

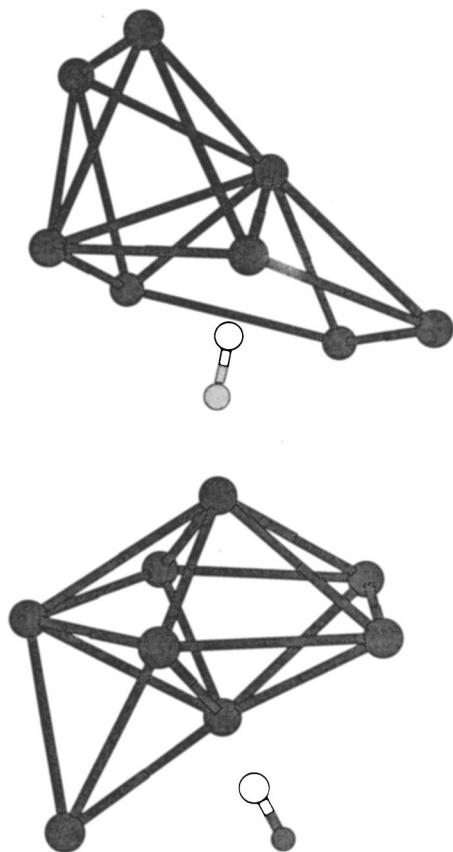


FIG. 9. Calculated isomeric structures of  $\text{Ar}_8\text{OH}$ : (top) minimum-energy (ME) structure ( $V_{8,1}$ ); (bottom) next higher isomer ( $V_{8,2}$ ), ME+17.41  $\text{cm}^{-1}$ . Their energies are given in Table I.

those of the respective  $\text{Ar}_{n+1}$  clusters, where the bottom Ar atom is substituted with OH. In fact, the same is true for the next higher isomers of  $\text{Ar}_8\text{OH}$  and  $\text{Ar}_9\text{OH}$ , shown in Figs. 9 (bottom) and 10 (bottom), respectively.

We mentioned earlier that the global minima of  $\text{Ar}_n\text{NO}$  clusters are also based on the optimal structures of  $\text{Ar}_{n+1}$ .<sup>44</sup> Nevertheless, for  $n=3-6$ , the minimum-energy structures of  $\text{Ar}_n\text{NO}$  differ from those of  $\text{Ar}_n\text{OH}$  clusters of the same size, since NO and OH generally do not replace the same Ar atom of  $\text{Ar}_{n+1}$ . Thus, in  $\text{Ar}_6\text{NO}$ , NO lies in the equator of the pentagonal bipyramid, while in  $\text{Ar}_6\text{OH}$ , OH occupies an axial site. Similarly,  $\text{Ar}_7\text{NO}$  has NO on the top of the bipyramid, in contrast to  $\text{Ar}_7\text{OH}$ , where OH is at the bottom.

For  $n \geq 7$ , the minimum-energy structures of  $\text{Ar}_n\text{CH}$  clusters closely resemble the most stable  $\text{Ar}_{n+1}$  configurations, though visibly distorted by the planar  $\text{Ar}_2\text{CH}$  motif.<sup>37</sup> However, while CH is solvated by a monolayer of all  $n$  Ar atoms, OH has only six Ar atoms in the first shell in this range of cluster sizes.

The strong similarity between the equilibrium geometries of  $\text{Ar}_n\text{OH}$  and  $\text{Ar}_n\text{HCl}$ ,<sup>46</sup> noted above for clusters with  $n=2-5$ , extends also to  $n=6-9$ .

#### 4. $\text{Ar}_n\text{OH}$ , $n=10-12$

The structure of the global minimum undergoes a dramatic change for  $n=10$ . Instead of partial solvation of OH by the  $\text{Ar}_6$  pentagonal pyramid, found for  $n=6-9$ ,  $\text{Ar}_{10}\text{OH}$

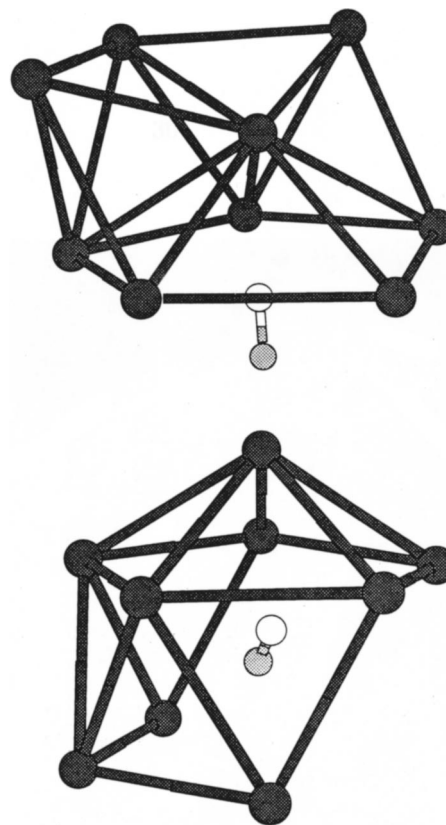


FIG. 10. Calculated isomeric structures of  $\text{Ar}_9\text{OH}$ : (top) minimum-energy (ME) structure ( $V_{9,1}$ ); (bottom) next higher isomer ( $V_{9,2}$ ), ME+11.78  $\text{cm}^{-1}$ . Their energies are given in Table I.

has the OH monomer at the center of an incomplete icosahedral cage formed by all ten Ar atoms [Fig. 11 (top)]. The lowest-energy structure of  $\text{Ar}_{11}\text{OH}$  in Fig. 12 (top) is one step closer to completion of the icosahedral Ar shell, with a single vacant site left. This vacancy is filled by adding the 12th Ar atom in  $\text{Ar}_{12}\text{OH}$ , whose global minimum corresponds to OH at the center of an  $\text{Ar}_{12}$  icosahedron [Fig. 13 (top)]. The icosahedral cage is slightly distorted, since the minimum-energy structure is calculated for a fixed orientation of OH. A dynamical treatment of  $\text{Ar}_{12}\text{OH}$  which would allow nearly free internal rotation of OH, as well as the relaxation of the argon cage, is expected to yield a virtually perfect OH-centered icosahedron.<sup>18</sup>

As was the case for smaller clusters, the minimum-energy structures of  $\text{Ar}_n\text{OH}$  for  $n=10-12$  can be obtained from those of  $\text{Ar}_{n+1}$ <sup>18,47,48</sup> by substituting the central Ar atom with OH. The next higher isomers of these clusters also derive from the global minima of  $\text{Ar}_{n+1}$ , this time by replacing an exterior Ar atom at the top of the pentagonal pyramid with OH [for  $\text{Ar}_{10}\text{OH}$ , this applies to the second local minimum  $V_{10,3}$  in Fig. 11 (bottom); the first local minimum  $V_{10,2}$  in Fig. 11 (middle) differs from the optimal  $n=10$  configuration only by a slight distortion of the Ar cage]. For  $n=10-12$ , Fig. 14 shows that the energy gap between the global and next higher local minima of  $\text{Ar}_n\text{OH}$  grows rapidly with increasing cluster size for  $n=10-12$  and peaks at  $n=12$ , demonstrating the great stability of icosahedral  $\text{Ar}_{12}\text{OH}$ .

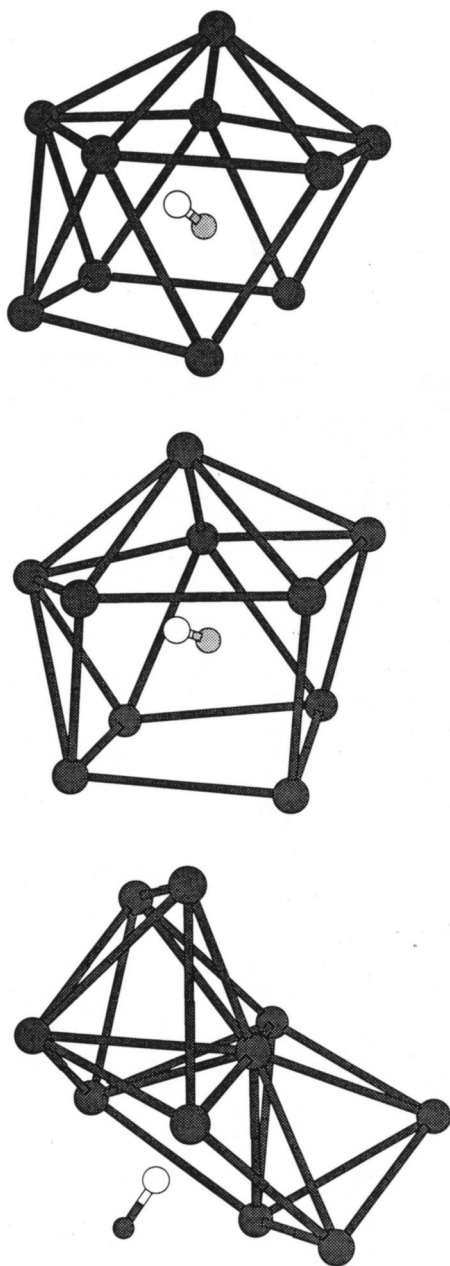


FIG. 11. Calculated isomeric structures of  $\text{Ar}_{10}\text{OH}$ : (top) minimum-energy (ME) structure ( $V_{10,1}$ ); (middle) next higher isomer ( $V_{10,2}$ ), ME + 16.13  $\text{cm}^{-1}$ ; (bottom) second close-lying isomer ( $V_{10,3}$ ), ME + 18.08  $\text{cm}^{-1}$ . Their energies are given in Table I.

In contrast to the fully solvated  $\text{Ar}_n\text{OH}$  structures, the lowest-energy isomers of  $\text{Ar}_n\text{NO}$  which are closely related to the global minima of  $\text{Ar}_{n+1}$ , have NO at a variety of surface sites of the Ar subunit.<sup>44</sup> The minimum-energy structures of  $\text{Ar}_{10}\text{CH}$  and  $\text{Ar}_{11}\text{CH}$  are analogous to those of their OH counterparts in Figs. 11 (top) and 12 (top), respectively.<sup>37</sup> However, the optimal  $\text{Ar}_{12}\text{CH}$  structure has CH at a surface site of the icosahedral shell, not in its center. In the global minima of  $\text{Ar}_n\text{HCl}$  clusters for  $n = 10-12$ , HCl also occupies a surface site of a partial or complete (for  $n = 12$ ) icosahedral Ar lattice.<sup>46</sup>

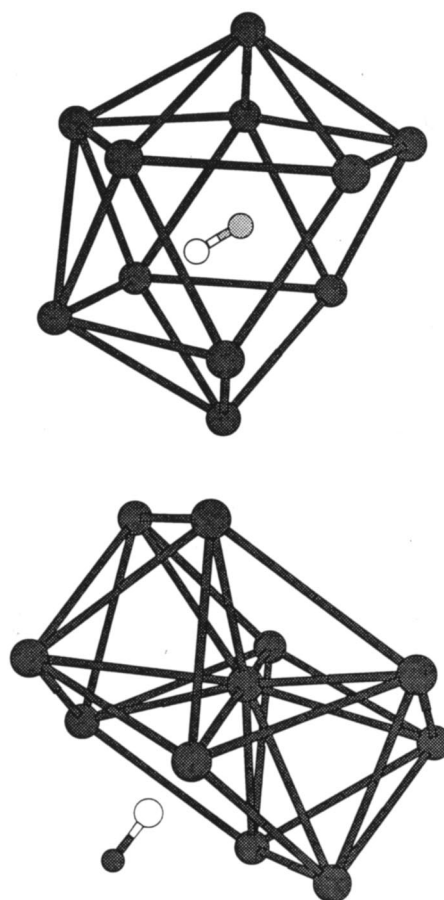


FIG. 12. Calculated isomeric structures of  $\text{Ar}_{11}\text{OH}$ : (top) minimum-energy (ME) structure ( $V_{11,1}$ ); (bottom) next higher isomer ( $V_{11,2}$ ), ME + 56.54  $\text{cm}^{-1}$ . Their energies are given in Table I.

### 5. $\text{Ar}_n\text{OH}$ , $n = 13-15$

The global minima of  $\text{Ar}_n\text{OH}$  for  $n = 13-15$ , displayed in Fig. 15, are generated by adding Ar atoms to the exterior of the icosahedral  $\text{Ar}_{12}\text{OH}$  [Fig. 13 (top)], thus initiating the second solvent shell around OH.

## IV. CONCLUSIONS

We have carried out simulated annealing calculations to find the global minimum and low-lying local minimum structures for  $\text{Ar}_n\text{OH}$  ( $X^2\Pi$ ) clusters with  $n = 1-15$ . The potential energy surfaces used take into account the open-shell nature of the OH ( $X^2\Pi$ ) molecule and spin-orbit coupling effects. Because of spin-orbit coupling, the Jahn-Teller effect is quenched and many of the minima are at high-symmetry geometries which would be forbidden in the absence of spin-orbit effects.

The  $\text{Ar}_n\text{OH}$  structures are generally similar to those found previously for the closed-shell  $\text{Ar}_n\text{HF}$  and  $\text{Ar}_n\text{HCl}$  clusters, but significantly different from those found for the open-shell  $\text{Ar}_n\text{NO}$  and  $\text{Ar}_n\text{CH}$  clusters. This is because the Ar-OH ( $X^2\Pi$ ) potential energy surface, like those for Ar-HF and Ar-HCl, has a near-linear equilibrium geometry. The  $A'$  and  $A''$  surfaces for Ar-OH are not sufficiently different to cause significant structural effects in the clusters.

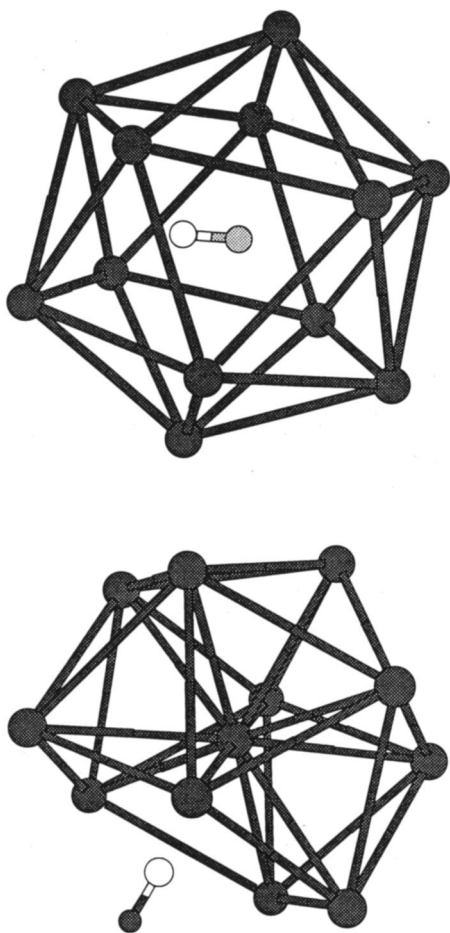


FIG. 13. Calculated isomeric structures of  $\text{Ar}_{12}\text{OH}$ : (top) minimum-energy (ME) structure ( $V_{12,1}$ ); (bottom) next higher isomer ( $V_{12,2}$ ), ME +  $86.29 \text{ cm}^{-1}$ . Their energies are given in Table I.

The Ar–NO and Ar–CH potential surfaces, by contrast, have T-shaped equilibrium geometries, and the resulting cluster structures are significantly different.

In a companion article,<sup>38</sup> we will use the structures determined here to carry out five-dimensional/two-surface (5D/

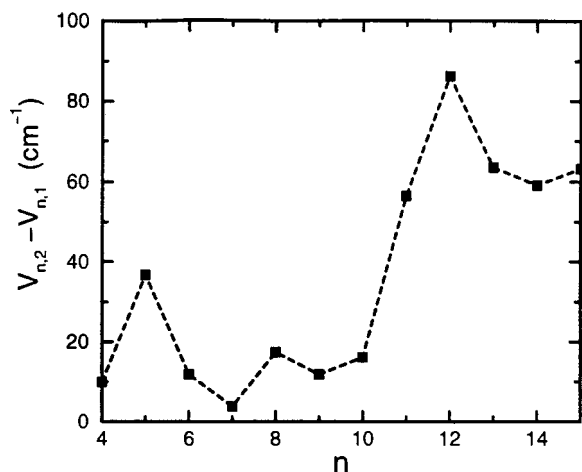


FIG. 14. Energy separation  $V_{n,2} - V_{n,1}$ , between the global ( $V_{n,1}$ ) and next higher local minimum ( $V_{n,2}$ ) of the  $\text{Ar}_n\text{OH}$  cluster, as a function of  $n$ , for  $n=4-15$ .

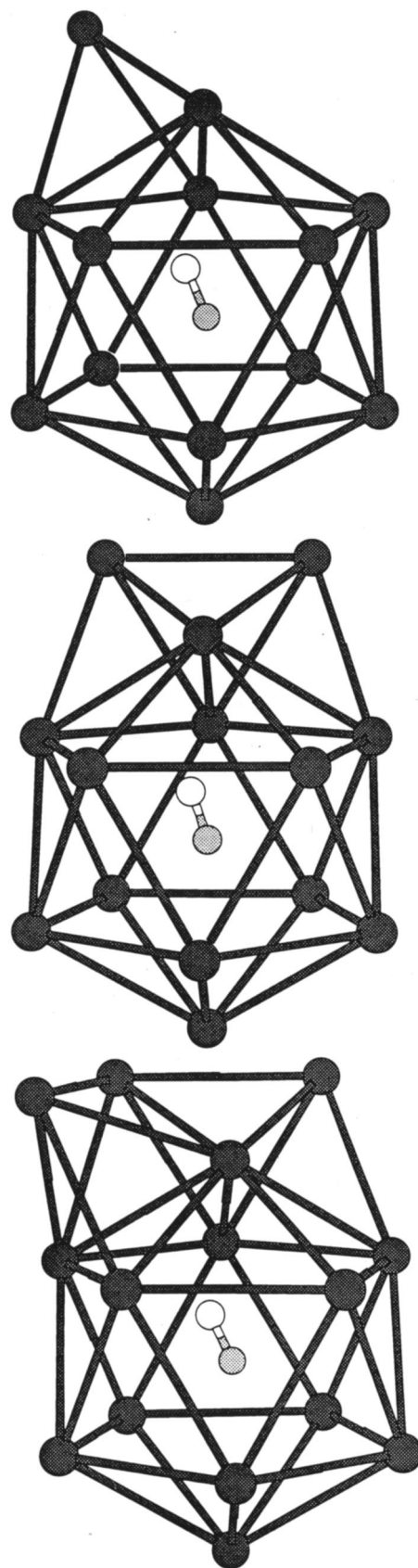


FIG. 15. Calculated minimum-energy structures: (top)  $\text{Ar}_{13}\text{OH}$  ( $V_{13,1}$ ); (middle)  $\text{Ar}_{14}\text{OH}$  ( $V_{14,1}$ ); (bottom)  $\text{Ar}_{15}\text{OH}$  ( $V_{15,1}$ ). Their energies are given in Table I.

2S) quantum dynamics calculations on the bound states of OH ( $X^2\Pi$ ) interacting with an Ar<sub>n</sub> subunit or cage.

## ACKNOWLEDGMENTS

Z.B. and M.X. have been supported in part by the National Science Foundation. Z.B. and M.X. also acknowledge the donors of the Petroleum Research Fund, administered by the ACS, for partial support of this research. J.M.H. is grateful to JILA, University of Colorado and National Institute of Standards and Technology, for hospitality during his Visiting Fellowship in 2001-2002.

- <sup>1</sup>S. J. Harris, S. E. Novick, and W. Klemperer, *J. Chem. Phys.* **60**, 3208 (1974).
- <sup>2</sup>T. A. Dixon, C. H. Joyner, F. A. Baiocchi, and W. Klemperer, *J. Chem. Phys.* **74**, 6539 (1981).
- <sup>3</sup>M. R. Keenan, L. W. Buxton, E. J. Campbell, A. C. Legon, and W. H. Flygare, *J. Chem. Phys.* **74**, 2133 (1981).
- <sup>4</sup>M. A. Dvorak, S. W. Reeve, W. A. Burns, A. Grushow, and K. R. Leopold, *Chem. Phys. Lett.* **185**, 399 (1991).
- <sup>5</sup>C. M. Lovejoy, M. D. Schuder, and D. J. Nesbitt, *J. Chem. Phys.* **85**, 4890 (1986).
- <sup>6</sup>G. T. Fraser and A. S. Pine, *J. Chem. Phys.* **85**, 2502 (1986).
- <sup>7</sup>Z. S. Huang, K. W. Jucks, and R. E. Miller, *J. Chem. Phys.* **85**, 6905 (1986).
- <sup>8</sup>C. M. Lovejoy and D. J. Nesbitt, *J. Chem. Phys.* **91**, 2790 (1989).
- <sup>9</sup>J. M. Hutson, *J. Chem. Phys.* **96**, 6752 (1992).
- <sup>10</sup>H. S. Gutowsky, T. D. Klots, C. Chuang, C. A. Schmuttenmaer, and T. Emilsson, *J. Chem. Phys.* **86**, 569 (1987).
- <sup>11</sup>A. McIlroy, R. Lascola, C. M. Lovejoy, and D. J. Nesbitt, *J. Phys. Chem.* **95**, 2636 (1991).
- <sup>12</sup>J. T. Farrell and D. J. Nesbitt, *J. Chem. Phys.* **105**, 9421 (1996).
- <sup>13</sup>J. T. Farrell, S. Davis, and D. J. Nesbitt, *J. Chem. Phys.* **103**, 2395 (1995).
- <sup>14</sup>C.-C. Chuang, S. N. Tsang, J. G. Hanson, W. Klemperer, and H.-C. Chang, *J. Chem. Phys.* **107**, 7041 (1997).
- <sup>15</sup>A. Ernesti and J. M. Hutson, *Phys. Rev. A* **51**, 239 (1995).
- <sup>16</sup>A. Ernesti and J. M. Hutson, *J. Chem. Phys.* **106**, 6288 (1997).
- <sup>17</sup>Z. Bačić, *J. Chem. Soc., Faraday Trans.* **93**, 1459 (1997).
- <sup>18</sup>S. Liu, Z. Bačić, J. W. Moskowitz, and K. E. Schmidt, *J. Chem. Phys.* **100**, 7166 (1994).
- <sup>19</sup>S. Liu, Z. Bačić, J. W. Moskowitz, and K. E. Schmidt, *J. Chem. Phys.* **101**, 6359 (1994).
- <sup>20</sup>S. Liu, Z. Bačić, J. W. Moskowitz, and K. E. Schmidt, *J. Chem. Phys.* **101**, 10181 (1994).
- <sup>21</sup>S. Liu, Z. Bačić, J. W. Moskowitz, and K. E. Schmidt, *J. Chem. Phys.* **103**, 1829 (1995).
- <sup>22</sup>P. Niyaz, Z. Bačić, J. W. Moskowitz, and K. E. Schmidt, *Chem. Phys. Lett.* **252**, 23 (1996).
- <sup>23</sup>H. Jiang, M. Xu, and Z. Bačić (unpublished).
- <sup>24</sup>J. M. Hutson, S. Liu, J. W. Moskowitz, and Z. Bačić, *J. Chem. Phys.* **111**, 8378 (1999).
- <sup>25</sup>C.-C. Chuang, S. N. Tsang, W. Klemperer, and H.-C. Chang, *J. Chem. Phys.* **109**, 484 (1998).
- <sup>26</sup>K. Nauta and R. E. Miller, *J. Chem. Phys.* **115**, 10138 (2001).
- <sup>27</sup>W. M. Fawzy and M. C. Heaven, *J. Chem. Phys.* **89**, 7030 (1988).
- <sup>28</sup>M. T. Berry, M. R. Brustein, J. R. Adamo, and M. I. Lester, *J. Phys. Chem.* **92**, 5551 (1988).
- <sup>29</sup>M. T. Berry, M. R. Brustein, and M. I. Lester, *J. Chem. Phys.* **90**, 5878 (1989).
- <sup>30</sup>W. M. Fawzy and M. C. Heaven, *J. Chem. Phys.* **92**, 909 (1990).
- <sup>31</sup>M. T. Berry, M. R. Brustein, and M. I. Lester, *J. Chem. Phys.* **92**, 6469 (1990).
- <sup>32</sup>M. T. Berry, M. R. Brustein, and M. I. Lester, *Chem. Phys. Lett.* **178**, 301 (1991).
- <sup>33</sup>M. T. Berry, R. A. Loomis, L. C. Giancarlo, and M. I. Lester, *J. Chem. Phys.* **96**, 7890 (1992).
- <sup>34</sup>Y. Ohshima, M. Iida, and Y. Endo, *J. Chem. Phys.* **95**, 7001 (1991).
- <sup>35</sup>R. T. Bonn, M. D. Wheeler, and M. I. Lester, *J. Chem. Phys.* **112**, 4942 (2000).
- <sup>36</sup>M. L. Dubernet and J. M. Hutson, *J. Chem. Phys.* **99**, 7477 (1993).
- <sup>37</sup>M. Xu, Z. Bačić, and J. M. Hutson, *Faraday Discuss.* **118**, 405 (2001).
- <sup>38</sup>M. Xu, Z. Bačić, and J. M. Hutson, *J. Chem. Phys.* **117**, 4787 (2002) (following paper).
- <sup>39</sup>K. P. Huber and G. Herzberg, *Molecular Spectra and Molecular Structure. IV. Constants of Diatomic Molecules* (Van Nostrand Reinhold, New York, 1979).
- <sup>40</sup>R. A. Aziz and H. H. Chen, *J. Chem. Phys.* **67**, 5719 (1977).
- <sup>41</sup>S. Liu, Z. Bačić, J. W. Moskowitz, and K. E. Schmidt, *J. Chem. Phys.* **101**, 8310 (1994).
- <sup>42</sup>C. J. Cerjan and W. H. Miller, *J. Chem. Phys.* **75**, 2800 (1981).
- <sup>43</sup>J. Nichols, H. Taylor, P. Schmidt, and J. Simons, *J. Chem. Phys.* **92**, 340 (1990).
- <sup>44</sup>F. Y. Naumkin and D. J. Wales, *Mol. Phys.* **98**, 219 (2000).
- <sup>45</sup>M. H. Alexander, S. Gregurick, P. J. Dagdigian, G. W. Lemire, M. J. McQuaid, and R. C. Sausa, *J. Chem. Phys.* **101**, 4547 (1994).
- <sup>46</sup>D. T. Anderson, S. Davis, and D. J. Nesbitt, *J. Chem. Phys.* **107**, 1115 (1997).
- <sup>47</sup>M. R. Hoare and P. Pal, *Adv. Phys.* **20**, 161 (1971).
- <sup>48</sup>M. R. Hoare and P. Pal, *J. Cryst. Growth* **17**, 77 (1972).